Detecting Wide Lines Using Isotropic Nonlinear Filtering

Laura Liu, David Zhang, *Senior Member, IEEE*, and Jane You, *Member, IEEE*

Abstract—Lines provide important information in images, and line detection is crucial in many applications. However, most of the existing algorithms focus only on the extraction of line positions, ignoring line thickness. This paper presents a novel wide line detector using an isotropic nonlinear filter. Unlike most existing edge and line detectors which use directional derivatives, our proposed wide line detector applies a nonlinear filter to extract a line completely without any derivative. The detector is based on the isotropic responses via circular masks. A general scheme for the analysis of the robustness of the proposed wide line detector is introduced and the dynamic selection of parameters is developed. In addition, this paper investigates the relationship between the size of circular masks and the width of detected lines. A sequence of tests has been conducted on a variety of image samples and our experimental results demonstrate the feasibility and effectiveness of the proposed method.

Index Terms—Curvilinear structures, feature extraction, isotropic nonlinear filter, line detection, wide line detector.

I. INTRODUCTION

THE analysis of images in the fields of pattern recognition and computer vision generally requires the detection of lines, also called curvilinear structures, from grayscale images. Line detection plays an important role for the success of higher level processing such as matching and recognition [1]–[6]. So far, many algorithms for line detection have been developed for different applications. The Hough transform [7]–[9], which is a widely used line detection method, was initially proposed to find analytically defined curvilinear structures (e.g., straight lines, circles, ellipses, etc.). Although the generalized Hough transform [10] can be used to detect arbitrary curvilinear structures in theory, it requires the complete specification of the exact shape of the curvilinear structure which is very difficult and even unfeasible for complex curvilinear structures in practice. One powerful approach is based on edge extraction and treats lines as objects with parallel edges [11]–[16]. An edge extraction algorithm [17] is first used to find all the edges in the image. The edge image is then analyzed to find the particular lines. However, the success of this approach depends on the accuracy of edges and the line thickness was not considered. Another popular approach is to use differential geometric properties to extract lines as ridges and valleys in the image [18]–[23]. A popular ridge detector [24] is based on the eigenvectors of the Hessian matrix which is given by the local second order derivatives. This detector extracts the ridges as points for which the intensities are maxima or minima in the main principal curvature direction, i.e., the direction of the maximum eigenvalue of the Hessian matrix. Nevertheless, this approach is sensitive to noise due to the use of second order of derivatives.

Although the line position detection is important, it would be useful if all the line's pixels (i.e., the pixels that comprise the full cross-sectional width) were also extracted. Koller *et al.* [25] presented an edge-based line finder for extracting line structures and their widths. This line finder employs the first derivative of Gaussian edge detectors and combines their outputs nonlinearly. This approach can detect lines of arbitrary widths by iterating in scale space and selecting as the line width the scale that yields the maximum of a scale-normalized response. However, due to the quantization of the scale space, this approach is computationally expensive and gives only a coarse estimate of the line width. Steger [26] proposed a ridge-based line detector which uses a line model with an asymmetrical profile to remove the bias of the line position as well as to extract the line width. This line detector overcomes the problem that the ridge-based line detection approach will return inaccurate line locations when the contrast on one side of the line is different from the contrast on the other side of the line. Moreover, since Gaussian masks are used to estimate the derivatives of the image, the line detector can scale to lines of arbitrary widths. Although this approach is useful for line width information detection, it has its limitations. Since this approach extracts lines as the maxima of the magnitude of the second directional derivatives, it can detect only salient lines. Also, once the selected σ becomes so large that neighboring lines start to influence each other, the line model will fail and the results will deteriorate.

The two line detection approaches, however, do not detect the whole of the line. A line, mathematically, is a 1-D figure without thickness, but an image line generally appears as a line of one or several pixels wide, i.e., as a thin/narrow or thick/wide line, having linear or curvilinear structures. In image processing and pattern recognition applications, line thickness or a line's full cross section is important in, for example, segmenting multiple orientation lines [27], in recognizing roads, railroads, or rivers from satellite or aerial imagery [11], [21], in extracting anatomical features in medical imaging for diagnoses [24], [28], [29],

and in detecting biometric traits for personal authentication [30]. It is, thus, important to detect not simply the line edges but rather *the whole of the line*.

In this paper, which has partly appeared in a preliminary form in [31], we present a robust method to detect the whole of the line, which we call the *wide line detector*. This wide line detector is implemented by employing a nonlinear filter without the use of any derivative. Isotropic responses are obtained by using circular masks which contain either a normalized constant weighting or a Gaussian profile. We restrict the sizes of circular masks so as to ensure that lines of different widths can be extracted in their entirety. We also design a line model which can analyze the robustness of the proposed wide line detector and which allows the automatic selection of parameters.

The paper is organized as follows. Section II introduces the line model and the relevant design issues. Section III presents the isotropic nonlinear filter based line detection method. In Section IV, we analyze the robustness of the proposed method and show how to automatically select parameters. Section V describes the results of our experiments. Section VI offers our conclusion.

II. MODEL DESIGN

In this section, we first introduce the models for line profiles in 1-D and then describe the design issues for the proposed line detection method with particular reference to 2-D line detection.

A. One-Dimensional Line Profile Model

Many line detection approaches model lines in 1-D as bar-shaped [25], i.e., the ideal line of width $2 \times w$ and height h is assumed to have a profile given by [26]

$$IL(x) = \begin{cases} h, & |x| \leq w \\ 0, & |x| > w \end{cases}. \tag{1}$$

However, the flatness of this profile is rarely found in real images. Generally speaking, in terms of different gray levels, there are three regions in a line image: the line part having a gray level Gr_{I}, the edge region having a gray level Gr_{II}, and the background having a gray level Gr_{III}. As an example, consider a bright line on a dark background, then we get $Gr_{\mathrm{I}} > Gr_{\mathrm{II}} > Gr_{\mathrm{III}}$. In this paper, therefore, a model for the common line profile in 1-D, the edge-based bar-shaped line, is defined as

$$GL(x) = h \times \begin{cases} 1, & |x| \leq w_l \\ b, & w_l < |x| < w_e \\ 0, & |x| > w_e \end{cases} \tag{2}$$

where $w_e > w_l > 0$ and $b \in [0, 1]$ and h is a scale or a vector, which represents height in the 1-D case and intensity in the 2-D case. For a bright line, also called a positive line, $h > 0$. For a dark line, also called a negative line, $h < 0$.

B. Two-Dimensional Line Detection

We now address the design issues for the proposed line detection method. Fig. 1 shows a dark line $(h < 0)$ in 2-D based on the 1-D ideal line model IL as in (1). A circular mask is shown at four image positions in Fig. 1. The detector groups pixels whose brightness is *similar* to the brightness at the center of the mask
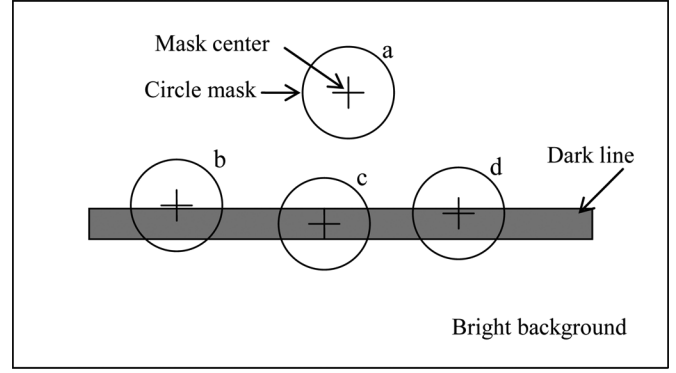
Fig. 1. Four circular masks at different positions on a line image based on the 1-D ideal line model IL as in (1).

into a *weighted mask having similar brightness* (WMSB). This similarity can be measured by

$$s(x, y, x_0, y_0, t) = \begin{cases} 1, & \text{if } |I(x,y) - I(x_0,y_0)| \leq t \\ 0, & \text{if } |I(x,y) - I(x_0,y_0)| > t \end{cases} \tag{3}$$

where (x_0, y_0) is the coordinate of the center, (x, y) is the coordinate of any other pixel within the mask, $I(x, y)$ is the brightness of the pixel (x, y), and t is the brightness contrast threshold. The summation of the outputs s within the circular mask gives the mass of WMSB. According to (3), when the center of the mask moves to a line on the image, the WMSB reaches the global maximum as the mask lies in a flat region of the image (as the mask a shown) and decreases when the center of the mask is very near a straight edge (as shown in the mask b) and decreases even further when very near the straight edge while remaining nonetheless in the line region (as shown in the mask d). Therefore, the smaller the WMSB mass, the larger the feature response. This is similar to the idea used for edge extraction and corner detection in [32]. Hence, to detect a line completely, the WMSB mass of any pixel on the line should be less than that of any background pixel.

Now let us consider a general situation: a line with an edge region in 2-D based on the common 1-D line profile GL as in (2). Fig. 2 provides an illustration in which a dark line is bounded by a gray band against a white background. In proximity to the lines are five circular masks. According to (3), in order to completely detect the line it is necessary that $|Gr_{\mathrm{I}} - Gr_{\mathrm{III}}| > t$. It is obvious that no matter what value b and h take in (2), the three different gray level regions (Fig. 3) have only four relations

$$\begin{array}{ll} \text{(i)} \begin{cases} |Gr_{\mathrm{I}} - Gr_{\mathrm{II}}| \leq t \\ |Gr_{\mathrm{II}} - Gr_{\mathrm{III}}| > t \end{cases} & \text{(ii)} \begin{cases} |Gr_{\mathrm{I}} - Gr_{\mathrm{II}}| > t \\ |Gr_{\mathrm{II}} - Gr_{\mathrm{III}}| > t \end{cases} \\ \text{(iii)} \begin{cases} |Gr_{\mathrm{I}} - Gr_{\mathrm{II}}| \leq t \\ |Gr_{\mathrm{II}} - Gr_{\mathrm{III}}| \leq t \end{cases} & \text{(iv)} \begin{cases} |Gr_{\mathrm{I}} - Gr_{\mathrm{II}}| > t \\ |Gr_{\mathrm{II}} - Gr_{\mathrm{III}}| \leq t \end{cases}. \end{array} \tag{4}$$

Now the question is how the edge region affects the WMSB mass of the line and the background pixels and thereby influences line detection. These matters will be considered in Section IV-B.

III. LINE DETECTION METHOD

The wide line detector is implemented to give isotropic line responses by applying a set of rules in a circular mask. Using
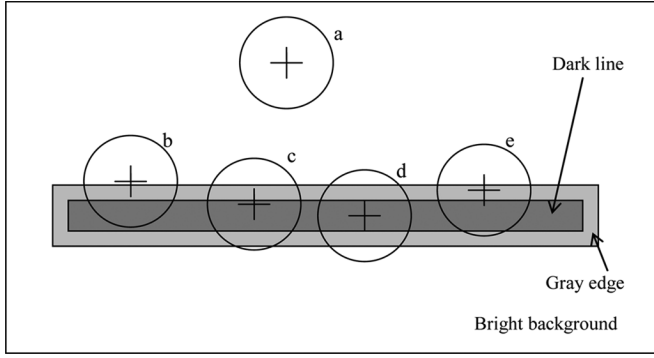
Fig. 2. Five circular masks at different positions of a line image based on the 1-D common line profile GL as in (2).
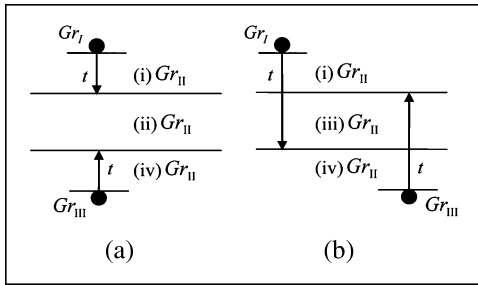
Fig. 3. Illustration of gray-level relations between three regions. Gr_I, Gr_{II}, and Gr_{III} are gray levels of the line part, the edge region, and the background, respectively. The difference of the gray levels between the line (Gr_I) and the background (Gr_{III}) is larger than the brightness contrast threshold t (a) with or (b) without larger than $2 \times t$; (i)–(iv) show the corresponding relations in (4), respectively.

a square kernel, the circular mask is digitally approximated to either with a constant weighting

$$\omega(x, y, x_0, y_0, r) = \begin{cases} 1, & \text{if } (x - x_0)^2 + (y - y_0)^2 \leq r^2 \\ 0, & \text{otherwise} \end{cases} \tag{5}$$

or with a Gaussian profile

$$\omega(x, y, x_0, y_0, r) = e^{-\frac{(x-x_0)^2 + (y-y_0)^2}{2r^2}} \tag{6}$$

where r is the radius of the circular mask. The normalization of the circular mask is obtained by the rule

$$\omega_0 = \frac{\omega}{\sum_{\substack{x_0 - r \leq x \leq x_0 + r, \\ y_0 - r \leq y \leq y_0 + r}} \omega(x, y, x_0, y_0, r)}. \tag{7}$$

As is usual when locally processing an image, the mask is centered on each pixel in the image and the brightness of any other pixel within the mask is compared with that of the center pixel. The comparison is determined by the rule defined in (3) along with a weighting function ω_0

$$c(x, y, x_0, y_0) = \omega_0(x, y, x_0, y_0, r) \times s(x, y, x_0, y_0, t) \tag{8}$$

TABLE I
DEVIATION OF FUNCTION $\sec h((I(x, y) - I(x_0, y_0))/t)^P$ FROM (3). HERE, c IS THE SUBTRACTION OF (11) FROM (3), AND $|c|$ IS THE ABSOLUTE VALUE OF c

P	c	$|c|$
2	2.6690	2.6690
3	1.0693	1.0693
4	0.4173	0.4173
5	**0.0705**	**0.0705**
6	-0.1427	0.1427
7	-0.2863	0.2863
8	-0.3893	0.3893
9	-0.4666	0.4666
10	-0.5264	0.5264

where c is the output of the weighting comparison. This comparison is done for each pixel within the mask. The WMSB mass of the center (x_0, y_0) is given by

$$m(x_0, y_0) = \sum_{\substack{x_0 - r \leq x \leq x_0 + r, \\ y_0 - r \leq y \leq y_0 + r}} c(x, y, x_0, y_0). \tag{9}$$

The initial line response L is the inverse WMSB mass obtained by

$$L(x_0, y_0) = \begin{cases} g - m(x_0, y_0) & \text{if, } m(x_0, y_0) < g \\ 0, & \text{otherwise} \end{cases}. \tag{10}$$

Here, g is the geometric threshold and $g = m_{\max}/2$, where $m_{\max}$ is the maximum value which m can take (usually $m_{\max} = \pi r^2$). The fixed threshold g for (10) is the theoretical optimum which is shown in the later analyses.

According to (3), the comparison s varies dramatically when a slight change of the brightness difference occurs very near the brightness contrast threshold t. In order to produce a smooth profile near the brightness contrast threshold, a hyperbolic secant function was used to give a much more stable and sensible version of (3) and is defined as

$$s(x, y, x_0, y_0, t) = \sec h\left(\frac{I(x, y) - I(x_0, y_0)}{t}\right)^5 \tag{11}$$

where $\sec h(x) = 2/(e^x + e^{-x})$. The use of the fifth power introduces the minimum difference from (3), as shown in Table I. This equation is plotted along with (3) in Fig. 4, where t is set to 10. It can be seen that, compared with (3), (11) produces a smoother profile and does not have too large an effect on s as a pixel's brightness changes slightly. This equation makes a tradeoff between stability about the threshold and the original requirement of the function, which is to take pixels having intensities similar to that of the center together into the mass of the circular mask.

Although the wide line detector is isotropic and can detect the whole of a line without the need to find the direction of line pixels, line direction is still necessary either for postprocessing or for application requirements. From (10), the direction of a
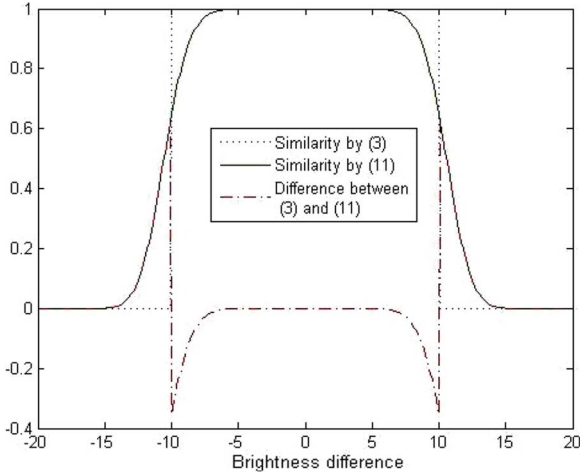
Fig. 4. Brightness difference versus the similarity functions defined in (3) and (11), respectively. Here, the brightness contrast threshold t is set to 10.

pixel with a nonzero line response is determined by finding the longest axis of symmetry

$$\phi = \begin{cases} \tan^{-1} \frac{y_m}{x_m}, & \text{if } d_m \geq 0 \\ -\tan^{-1} \frac{y_m}{x_m}, & \text{otherwise} \end{cases} \tag{12}$$

$$x_m = \sum_{\substack{x_0 - r \leq x \leq x_0 + r, \\ y_0 - r \leq y \leq y_0 + r}} (x - x_0)^2 c(x, y, x_0, y_0) \tag{13}$$

$$y_m = \sum_{\substack{x_0 - r \leq x \leq x_0 + r, \\ y_0 - r \leq y \leq y_0 + r}} (y - y_0)^2 c(x, y, x_0, y_0) \tag{14}$$

$$d_m = \sum_{\substack{x_0 - r \leq x \leq x_0 + r, \\ y_0 - r \leq y \leq y_0 + r}} (x - x_0)(y - y_0) c(x, y, x_0, y_0) \tag{15}$$

where $\phi \in (-(\pi/2), (\pi/2)]$. The value of ϕ is exactly correct only for lines parallel to one of the coordinate axes or at an angle of $\pi/4$ to a coordinate axis. In other cases, deviations of the calculation of ϕ will occur. However, such deviation of ϕ from the line orientation is small and can be ignored.

In some cases, only dark or bright lines are required, for example, with reference to blood vessels in X-ray images (dark lines generally required) and aerial images (bright lines generally required). Introducing a step function, $\Theta(\Delta)$, we can implement the wide line detector to extract bright or dark lines according to need

$$s(x, y, x_0, y_0, t) = \sec h \left(\frac{\Delta \Theta(\Delta)}{t} \right)^5 \tag{16}$$

where $\quad \Theta(\Delta) \quad = \quad \begin{cases} 1, & \Delta > 0 \\ 0, & \text{else} \end{cases} \quad$ and

$\Delta = \begin{cases} I(x, y) - I(x_0, y_0), & \text{if dark line} \\ I(x_0, y_0) - I(x, y), & \text{if bright line.} \end{cases}$

IV. PARAMETER SELECTION

The proposed line detection method requires two parameters—the radius of the circular mask r and the brightness contrast threshold t. In this section, we provide analyses to show

how the two parameters affect the line detection result and then present approaches for automatically selecting the two parameters so that the proposed method is robust.

A. Radius of Circular Mask, r

Obviously, complete line detection requires that the circular mask should at least be bigger than the line width. The radius of the circular mask r must, therefore, be restricted so as to ensure that the whole of the line can be detected using the inverse WMSB mask. In this section, we analyze the relationship between the radius of a circular mask r and the width of the line detected $2 \times w$, first with regard to circular masks with a normalized constant weighting, and then those with a Gaussian profile.

1) Circular Mask With Normalized Constant Weighting: In this section, we employ the line mode IL to discuss the relationship between the size of circular mask with constant weighting and the width of detected line.

Definition 1: Given an image region I and a line L of width $2 \times w$, for any given point $p \in I$, *the distance of p to L, d_p^L, is* defined by the rule

$$d_p^L = \min \{ d(p, p_{L_m}) | \forall p_{L_m} \in L_m,$$
$$d(p, p_{L_m}) = \sqrt{(x_p - x_{p_{L_m}})^2 + (y_p - y_{p_{L_m}})^2} \} \tag{17}$$

where L_m is the middle axis of L in the line direction.

Definition 2: Let C denote a circle region with radius r in an image. *The mass of point p_0, the center of the circle region, is* defined as

$$M_{p_0} = \iint_C s_p dx dy \tag{18}$$

$$s_p = \begin{cases} 1, & \text{if } |I_p - I_{p_0}| \leq t \\ 0, & \text{if } |I_p - I_{p_0}| > t \end{cases} \tag{19}$$

where p is any other point in the circle region C and I_p is the intensity of point p.

Proposition 1: Denote the background $B = \{(x, y) | (x, y) \in I, (x, y) \notin L\}$. For each $p_l \in L$, $p_b \in B$, if $|I_{p_l} - I_{p_b}| > t$, there exist the following.

1) M_{p_l} is monotonically decreasing relative to $d_{p_l}^L$ and $M_{p_L} = \max\{M_{p_l} | p_l \in L\}$ for each $p_L \in L_m$.
2) M_{p_b} is monotonically increasing relative to $d_{p_b}^L$ and $M_{p_B} = \min\{M_{p_b} | p_b \in B\}$ for each $p_B \in \{p_b | d_{p_b}^L = w\}$.

Proof: Assume that the center of circular region C is the coordinate origin. Rotate the coordinate axes about the origin so that the y axis is parallel to L_m, as shown in Fig. 5. We define $w_1 = |x_{p_1}|$ and $w_2 = |x_{p_2}|$, where $x_{p_1} = \max\{x_p | p \in C \cap L\}$ and $x_{p_2} = \min\{x_p | p \in C \cap L\}$ are the x coordinates of the right- and left-most intersection points of the circle region C and the line L, respectively. As there exists $|I_{p_l} - I_{p_b}| > t$, for each $p_l \in L$, $p_b \in B$, according to (18) and (19), we can get $M_{p_l} = \iint_{C \cap L} 1 dx dy$ and $M_{p_b} = \iint_{C \cap B} 1 dx dy$.

1) For each $p_l \in L$, when the circle C is centered on p_l [as shown in Fig. 5(a)], we have (20), shown at the bottom
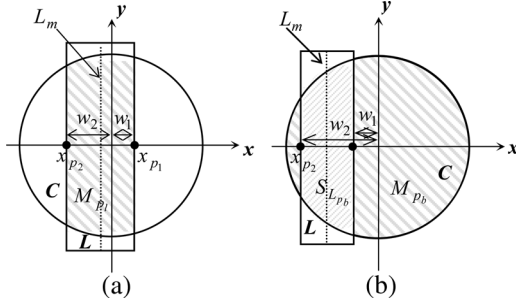
Fig. 5. Illustration of Proposition 1 and its proof.

of the page, where $0 \leq w_1 \leq w$. For convenience, denote

$$f(x) = \arcsin x + x\sqrt{1 - x^2} \tag{21}$$

where $0 \leq x \leq 1$. Then, the (20) can be rewritten as

$$M_{p_l} = \begin{cases} r^2 \left[f(x) + f\left(\frac{2w}{r} - x\right) \right], & x > \frac{2w}{r} - 1 \\ r^2 \left[f(x) + \frac{1}{2}\pi \right], & x \leq \frac{2w}{r} - 1 \end{cases}$$

where $x = w_1/r$. It is obvious that the derivative $M'_{p_l} \geq 0$. Therefore, M_{p_l} is monotonically decreasing relative to $d^L_{p_l}$. Hence, when $p_L \in L_m$, $d^L_{p_L} = 0$ and M_{p_L} takes the maximum value

$$M_{p_L} = 2r^2 f\left(\frac{w}{r}\right). \tag{22}$$

2) For each $p_b \in B$, when the circle C is centered on p_b [as shown in Fig. 5(b)], we have $M_{p_b} = \iint\limits_{C \cap B} 1 dx dy = \pi r^2 - S_{L_{p_b}}$ and

$$S_{L_{p_b}} = \int_{x_{p_2}}^{x_{p_1}} \int_{-\sqrt{r^2 - x^2}}^{\sqrt{r^2 - x^2}} 1 dx dy$$

$$= r^2 \arcsin \frac{x}{r} + x\sqrt{r^2 - x^2} \Big|_{w_1}^{w_2}$$

$$= \begin{cases} r^2 \left[\frac{1}{2}\pi - f(x) \right], & x \geq 1 - \frac{2w}{r} \\ r^2 \left[f\left(\frac{2w}{r} + x\right) - f(x) \right], & x < 1 - \frac{2w}{r} \end{cases}$$

where $x = w_1/r$. It is obvious that $S'_{L_{p_b}} < 0$. Therefore, M_{p_b} is monotonically increasing relative to $d^L_{p_b}$. Hence, for each $p_B \in \{p_b | d^L_{p_b} = w\}$, $d^L_{p_b}$ reaches the minimum value w, and M_{p_b} takes the minimum value

$$M_{p_B} = \begin{cases} \frac{1}{2}\pi r^2, & r \leq 2w \\ r^2 \left[\pi - f\left(\frac{2w}{r}\right) \right], & r > 2w \end{cases}. \tag{23}$$

□

The meaning of Proposition 1 is that, no matter what size of the circular mask, the smaller the distance of the pixel to L, the larger the WMSB mass if the pixel is on the line, while the smaller the WMSB mass if the pixel on the background. Consequently, pixels on the middle axis of a line take the local maximum value of the WMSB mass, whereas pixels on the background very near the edges of the line take the local minimum WMSB mass. As mentioned in Section II-B, in order to detect a line completely, the maximum of the WMSB mass that the line pixel can take should be less than the minimum that the background pixel can take. Therefore, according to Proposition 1 and its proof, from (22) and (23), we get

$$\begin{cases} 2f(x) + f(2x) < \pi, & 0 < x < \frac{1}{2} \\ 2f(x) < \frac{1}{2}\pi, & \frac{1}{2} \leq x < 1 \end{cases} \tag{24}$$

where $x = w/r$.

Fig. 6 illustrates the inequality relations defined by (24). We can see that only $x \leq 0.43$ meets the inequality. Given the line width, the smaller the x value, the larger the mask size r. There is a tradeoff to be made here as a smaller ratio means a slower detection yet the use of a larger ratio, and, therefore, a smaller mask will undermine line detection. Hence, we set $x_0 = 0.4$ by experience. The relationship between the width of detected line, $2 \times w$, and the radius of a constant weighting circular mask, r, is

$$r \geq 2.5w. \tag{25}$$

According to (22), the maximum of WMSB mass which line pixels can take is $M_{p_L} = 2r^2 f(x_0)$. Therefore, the geometric threshold g used in (10) is equal to $g = 2r^2 f(x_0)/\pi r^2 = 2f(x_0)/\pi \approx 0.5$.

$$M_{Pl} = \int_{x_{P2}}^{x_{P1}} \int_{-\sqrt{r^2 - x^2}}^{\sqrt{r^2 - x^2}} 1 dy dx$$

$$= 2\int_0^{w_1} \sqrt{r^2 - x^2} dx + 2\int_0^{w_2} \sqrt{r^2 - x^2} dx$$

$$= \begin{cases} r^2 \left[\arcsin \frac{w_1}{r} + \frac{w_1}{r}\sqrt{1 - \left(\frac{w_1}{r}\right)^2} \right. \\ \qquad \left. + \arcsin \frac{2w - w_1}{r} + \frac{2w - w_1}{r}\sqrt{1 - \left(\frac{2w - w_1}{r}\right)^2} \right], & w_1 > 2w - r \\ r^2 \left[\arcsin \frac{w_1}{r} + \frac{w_1}{r}\sqrt{1 - \left(\frac{w_1}{r}\right)^2} \right] + \frac{1}{2}\pi r^2, & w_1 \leq 2w - r \end{cases} \tag{20}$$
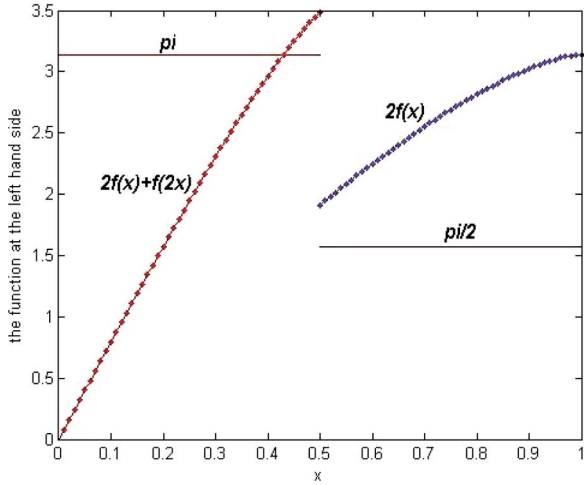
Fig. 6. Illustration of the inequality relation about the ratio of the width of the line detected to the radius of a circle mask with normalized constant weighting.

TABLE II
RELATIONSHIP BETWEEN RADII OF GAUSSIAN MASKS AND APPROXIMATELY CRITICAL WIDTHS OF LINES (ACLW) DETECTED

Radius of Gaussian mask	ACLW	Digital ACLW
3	2.6	2
4	3.5	3
5	4.4	4
6	5.3	5
7	6.2	6
8	7.1	7
9	7.9	8
10	8.8	9
11	9.7	10
12	10.6	10
13	11.5	11
14	12.4	12
15	13.2	13

2) Circular Mask With Gaussian Profile: Now we discuss the relationship between the width of the line detected and the size of a circular mask with a Gaussian profile. Although Proposition 1 is for a constant weight, it is evident that we can get the same conclusion for a Gaussian weight. That is, the WMSB area of a line reaches a local maximum when the line passes through the center of the circular mask. Assume that a circle C with a radius r has a density $e^{-((x^2+y^2)/2r^2)}$ and a line of width $2 \times w$ traverses the center of the circle. Let L_C denote the part of the line within the circle. According to the definition of line response [see (10)], if a line of width $2 \times w$ is to be completely detected by using a Gaussian mask with radius r, it requires

$$\iint\limits_{L_C} e^{-\frac{x^2+y^2}{2r^2}} dxdy < \frac{1}{2} \iint\limits_{C} e^{-\frac{x^2+y^2}{2r^2}} dxdy \qquad (26)$$

which is equivalent to

$$\int_0^w \int_0^{\sqrt{r^2-x^2}} e^{-\frac{x^2+y^2}{2r^2}} dxdy < \frac{1}{2} \int_0^r \int_0^{\sqrt{r^2-x^2}} e^{-\frac{x^2+y^2}{2r^2}} dxdy. \qquad (27)$$

The right hand side can be simplified as

$$\int_0^r \int_0^{\sqrt{r^2-x^2}} e^{-\frac{x^2+y^2}{2r^2}} dxdy = \int_0^{\frac{\pi}{2}} d\theta \int_0^r e^{-\frac{\rho^2}{2r^2}} \rho d\rho$$
$$= \frac{\pi}{2} r^2 (1 - e^{-1/2}). \qquad (28)$$

Therefore

$$\int_0^w \int_0^{\sqrt{r^2-x^2}} e^{-\frac{x^2+y^2}{2r^2}} dxdy < \frac{\pi}{4} r^2 (1 - e^{-1/2}). \qquad (29)$$

This equation determines the relationship between the width of the line detected and the radius of a circular mask with a Gaussian profile. Given a mask with a radius r, the critical width of the line detected is obtained when the left and right arguments of (29) are equal. As the analytic form of the left function is not available, we provide only the approximate critical width

of the line detected as shown in Table II, as well as the corresponding digital approximations. Therefore, given a Gaussian profile mask of radius r, a line is definitely detected if it is not wider than the digital approximation of the corresponding critical width.

B. Brightness Contrast Threshold, t

Ideally, a line is defined as the profile of two distinctive regions as described in Section II-A (see Fig. 1). However, in general, there are shaded areas between the two distinctive regions, as shown in Fig. 2. Here, we call such area as the *edge region*. Therefore, we have to take into account the influence of the edge region on the WMSB mass, which is related to the brightness contrast threshold that defines the minimum contrast of the detected features. In this section, we first analyze the relationship between the brightness contrast threshold and the WMSB mass and then give the automatic selection of a proper t.

Proposition 2: Given a line L of width $2 \times w$ bounded by an edge region of width e denoted by $E = \{(x,y)|(x,y) \in I, w \leq d_{(x,y)}^L \leq w + e, e \ll w\}$ and a circle C of radius r with the constraint $w \leq 0.4r$. Define the background $B = \{(x,y)|(x,y) \in I, (x,y) \notin L \cup E\}$. For each $p_l \in L, p_e \in E, p_b \in B$, if 1) $|I_{p_l} - I_{p_b}| > t$ and 2) $M_{p_l} < M_{p_b}$, there exists $\begin{cases} M_{p_e} < M_{p_l} & if \ |I_{p_e} - I_{p_b}| > t \\ M_{p_e} > M_{p_l} & otherwise \end{cases}$. Here, the sign "$\ll$" means much less than.

Proof: From Proposition 1, condition 2) can be rewritten as $M_{p_L} < M_{p_B}$. As discussed in Section II-B, there are only four relations between three different gray-level regions.

Case 1) $|I_{p_e} - I_{p_b}| > t$ and $|I_{p_l} - I_{p_e}| \leq t$. Suppose $L' = L \cup E$, then L' is a line with a width of $2 \times (w + e)$ and $L'_m = L_m$. According to Definition 1, we always have $d_{p_l}^{L'} < d_{p_e}^{L'}$. From Proposition 1, for each $p_{l'} \in L'$, $M_{p_{l'}}$ is monotonically decreasing relative to $d_{p_{l'}}^{L'}$. Therefore, for each $p_l \in L, p_e \in E, p_b \in B$, we get $M_{p_e} < M_{p_l} < M_{p_b}$.

Case 2) $|I_{p_e} - I_{p_b}| > t$ and $|I_{p_l} - I_{p_e}| > t$. From Proposition 1, for each $p_l \in L$, when $p_l \rightarrow E^- =$
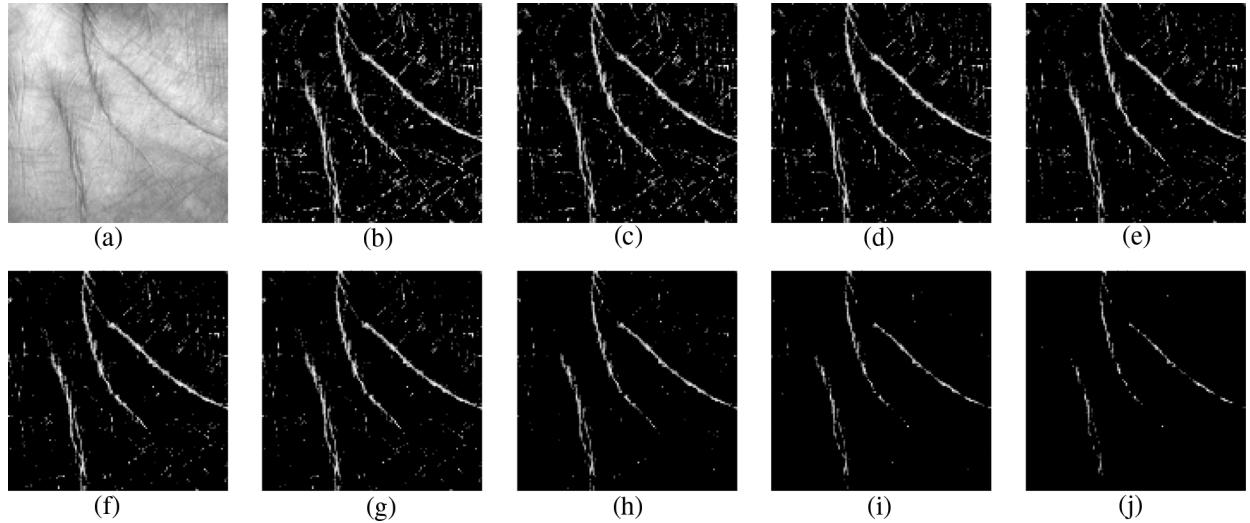
Fig. 7. (a) Segmented palmprint image. Palm-line response images obtained using brightness contrast thresholds t of (b) 6, (c) 7, (d) 8, (e) 9, (f) 10, (g) 11, (h) 15, (i) 20, and (j) 25.

$\{(x,y)|d^L_{(x,y)} = w\}$, $d^L_{p_l}$ approaches the maximum value w, and M_{p_l} reaches the minimum value $M_{p_{E-}} = r^2 f(2w/r)$. From $e \ll w$, we always get $\max(M_{p_e}) < M_{p_{E-}} = \min(M_{p_l})$. Therefore, for each $p_l \in L$, $p_e \in E$, $p_b \in B$, we have $M_{p_e} < M_{p_l} < M_{p_b}$.

Case 3) $|I_{p_e} - I_{p_b}| \leq t$ and $|I_{p_l} - I_{p_e}| \leq t$. According to (18) and (19), we have $M_{p_e} = \iint_C 1 dx dy = \pi r^2$. Obviously, for each $p_l \in L$, $p_e \in E$, $p_b \in B$, we always have $M_{p_l} < M_{p_b} \leq M_{p_e}$.

Case 4) $|I_{p_e} - I_{p_b}| \leq t$ and $|I_{p_l} - I_{p_e}| > t$. Based on Proposition 1, when $d^L_{p_l} = 0$, M_{p_l} takes the maximum value $M_{p_L} = 2r^2 f(w/r)$. Suppose $B' = B \cup E$, then for each $p_{b'} \in B'$, when $p_{b'} \to E^+ = \{(x,y)|d^L_{(x,y)} = w+e\}$, $d^L_{p_{b'}}$ reaches the minimum w, $M_{p_{b'}}$ takes the minimum value $M_{p_{E+}} = r^2[\pi - f(2w/r)]$. Owing to $w \leq 0.4r$, from Fig. 6, we can get $M_{p_L} < M_{p_{E+}}$. Therefore, for each $p_l \in L$, $p_e \in E$, $p_b \in B$, we have $M_{p_l} < M_{p_e} < M_{p_b}$.

Hence, from Cases 1) and 2), if $|I_{p_e} - I_{p_b}| > t$, we have $M_{p_e} < M_{p_l}$; from Cases 3) and 4), if $|I_{p_e} - I_{p_b}| \leq t$, we have $M_{p_e} > M_{p_l}$.   □

From Proposition 2 and its proof, we conclude that for a given image, if the contrast between the edge region and the background is less than the threshold t, the edge region *can be* regarded as one part of the line; otherwise, the edge region *must be* regarded as one part of the line. That is, for a given image, a large brightness contrast threshold *may* result in a "narrow" line being detected, while a small brightness contrast threshold *must* result in a "broad" line being detected. Therefore, the brightness contrast threshold t qualitatively determines the width of lines detected.

Fig. 7 gives an example of line response images with different t. Here, dark line pixels are extracted directly from the input segmented palmprint image [see Fig. 7(a)] by using a constant weighting mask with a radius of 8 pixels. It can be seen that as the brightness contrast threshold increases, the number of false response pixels and true response pixels are both decrease. It is,

thus, necessary to select a proper t to guarantee the detection of the whole line. By experience, we defined t as

$$t = round(std(I)) \tag{30}$$

where std is the standard deviation function, $round$ means the nearest integer, and I is the input image. According to (30), the brightness contrast threshold t used in Fig. 7(a) is 9.

V. EXPERIMENTAL RESULTS

Our line detection method is implemented for the synthesized image and real images in several different applications to completely detect lines of different widths. For the purpose of establishing the effectiveness and robustness of our line detection method, the output images of our wide line detector are compared with those of line detection approaches based on edge extraction [25] and ridge detection [26], which are designed to extract the line width along with the line position. For speed, the *sech* to the fifth power formula in (11) is implemented using a look up table.

A. Synthesized Image

We synthesized an image including straight lines and curves (curvilinear structures) with different widths and different intensities. Fig. 8(a) shows the synthesized image. Applying the proposed wide line detector we obtain the result shown in Fig. 8(d). Here, we employed the core function defined in (11). The brightness contrast threshold used is 11 according to (30). The maximum width in Fig. 8(a) is 5, and, thus, the operating radius of circular mask is 7 according to (25). Fig. 8(b) and (c) shows the line detection results by the edge-based line finder [25] and the ridge-based line detector [26], respectively. Since our method detects lines based on extracting the whole line while the other two approaches detect lines based on detecting the corresponding edges of each line pixel, we show the line detection result in the corresponding way, as shown in Fig. 8(b)–(d). It can be seen that the line detection results
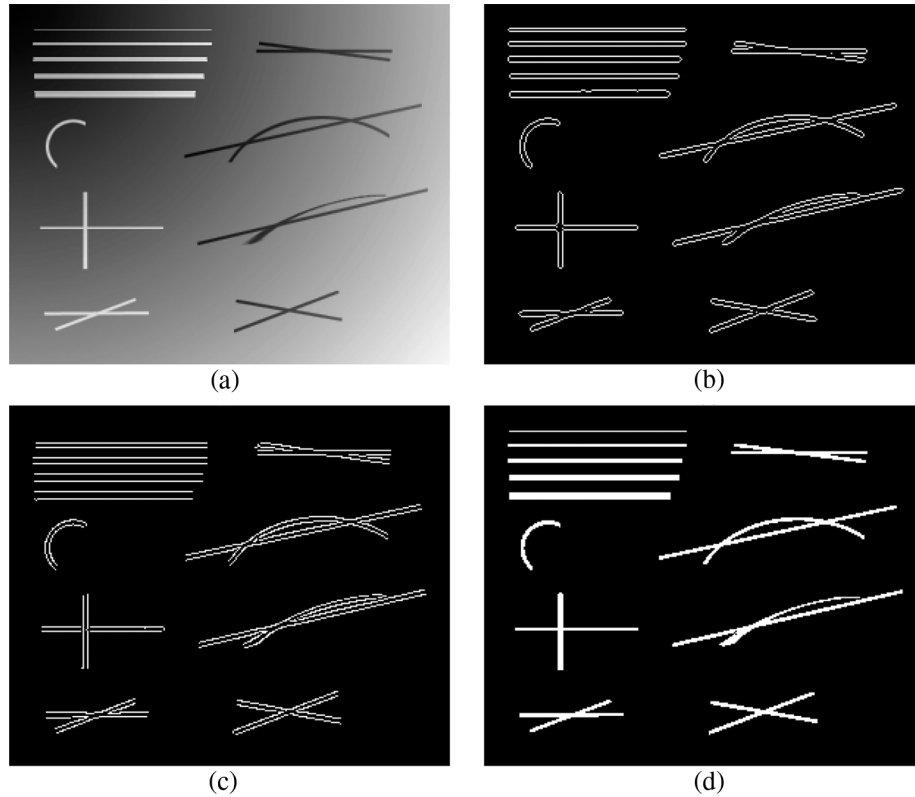
Fig. 8. (a) Test image including straight lines and curves of different widths. The line detection results obtained using (b) the edge-based line finder, (c) the ridge-based line detector, and (d) the proposed wide line detector.

by using our method is more accurate than that obtained by using either the edge-based line finder or the ridge-based line detector.

B. Real Images

Fig. 9(a)–(c) is taken from [26] including two aerial images and one X-ray image. Fig. 9(g)–(i) shows the line detection results obtained using our wide line detector. The brightness contrast threshold for each input image is calculated by (30). A circular mask with a normalized constant weighting is used for each input image to detect lines and the corresponding radius of the circular mask is determined according to (25) based on the width of the widest line expected to be detected. In postprocessing, we discarded very short linear structures (<10 pixels) and very "rounded" line structures (the eccentricity <0.75). Fig. 9(d)–(f) displays the corresponding line extraction results reported in [26].

Fig. 9(d) shows the line detection result obtained by using the ridge-based line detector. We can see that the unjustified edge points are reported in the junction area because the line width here exceeds the range of widths that can be detected and, further, that the estimation of the line width of the road object in the bottom of the image is too large due to the effect of the nearby vegetation. Fig. 9(g) shows the corresponding line detection result obtained by using our wide line detector. It can be seen that the method is able to correctly detect the wide lines (i.e., essentially all the pixels that comprise line cross-sectional extents), even at the junction area in the middle of the image and the

road close to vegetation in the bottom part of the image (see red circles).

The aerial image at Fig. 9(b) is more of a challenge. It contains a large area where the model of the line does not hold, but as can be seen in Fig. 9(h), our wide line detector nonetheless works well. Because bright lines are needed here, we employed the (16) as the core function of the wide line detector to suppress the dark-line response. Comparing the line detection results obtained by the ridge-based line detection approach [see Fig. 9(e)] and our method, we can see that the narrow line in the left upper part, which has a width close to two, is extracted correctly by using our method, while the corresponding line detected in Fig. 9(e) is not fully extracted as its cross-sectional extent is too narrow at some positions. Further, the wide line in the right upper part of the image is detected completely in Fig. 9(h), while it is missed in Fig. 9(e).

Fig. 9(c) is a low contrast X-ray image. Fig. 9(f) and (i) shows the line detection results by using the ridge-based line detector and our method, respectively. It can be seen that our method certainly performs as well as the ridge-based line detector in delineating the vascular stenosis in the central part, and is also able to detect some very narrow and thin arteries (see red circles) which do not appear in Fig. 9(f).

The next example, Fig. 10, which shows four segmented 128× 128 palmprint images (the first row), is from the domain of biometrics. There are a number of reasons for employing palmprint images to test our line detection method: 1) palm lines, referring to principal lines and wrinkles [30], are negative
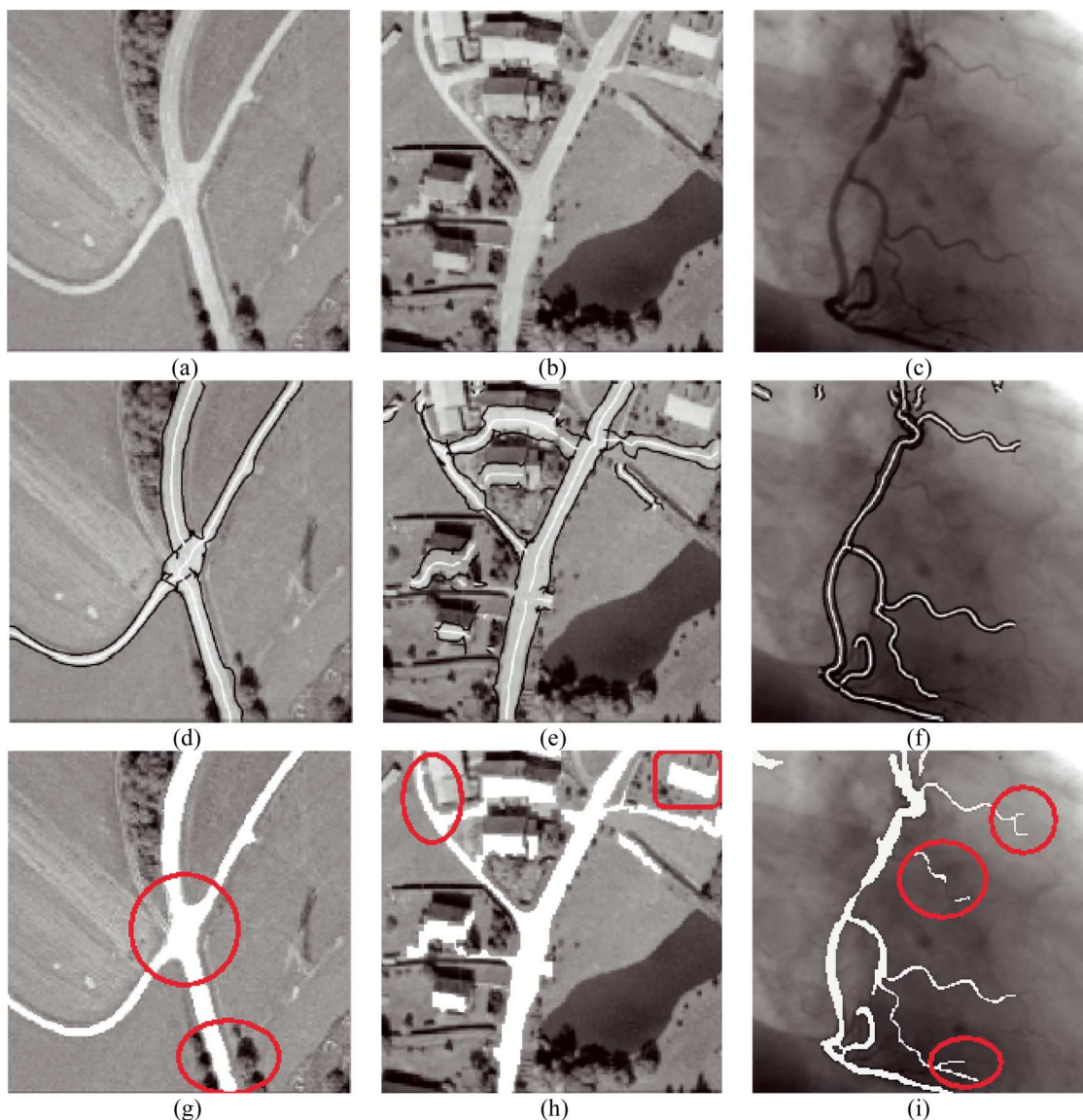
Fig. 9. (a), (b) Aerial images and (c) an X-ray image taken from [26]. (d)–(f) Extraction results of line positions and line widths reported in [26] where line positions are displayed in white with the corresponding edges displayed in black. (g)–(i) Corresponding line detection results obtained using our wide line detector are drawn in white.

lines of varying widths; 2) there are many details on palm lines such as corners, junctions and branches; 3) some palmprints contain complex structures along with different line widths, as shown in the last image of the first row. This example compares the line detection results by using our method (see the last row) with those by the edge-based line finder (see the second row) and the ridge-based line detector (see the third row), all of which are displayed in black. We can see that all three line detectors can extract the principal lines well, however, our method better detects details such as the ellipse on the principal line in the first column image (see the red circle), the intersection of two thin lines in the right parts of images of the middle two columns (see the red circles), and the branches on the principal lines in the last column image (see red rectangles). Further, our line detection method also outperforms the two other approaches for the last column image, which contains complex palm lines.

Fig. 11 displays three segmented tongue images in the first row, which followed by the output images of the edge-based line finder (the second row), the ridge-based line detector (the third row) and our wide line detector (the last row), respectively. The line detection results are all displayed in red. In the first column image, there is a crackle, which refers to a dark line in a tongue image, very thick and broad. Our line detection method extracts this crackle correctly (see yellow circles), whereas the other two approaches not only fail to correctly extract this crackle but, because the width of the crackle varies greatly, miss branches of the crackle. In the middle column, the most salient crackle in the middle of the image has an irregular structure, especially in the upper part where the width of the crackle changes dramatically and becomes discontinuous. Again, only our method correctly extracts the wide line and the interruption to the line (see the yellow circle). The other two approaches produce unjustified edge points, and a misleadingly continuous line. The last tongue
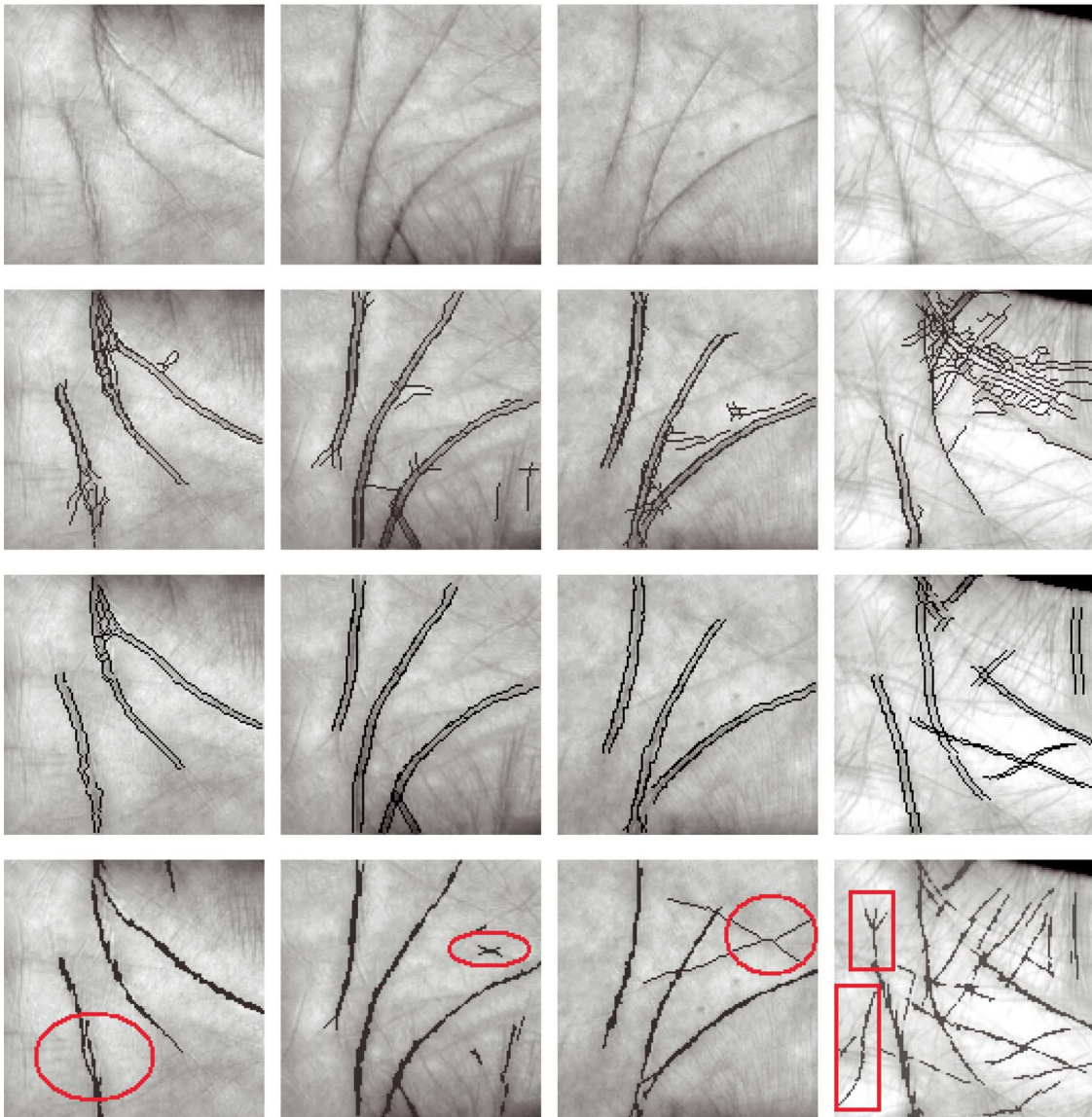
Fig. 10.   Segmented (first row) palmprint images and (second row) the palm-line detection results obtained using the edge-based line finder, (third row) the ridge-based line detector, and (last row) our wide line detector. Detected lines are displayed in black.

image is the most difficult because it is low contrast and contains many line segments of different thicknesses and widths. Comparing the corresponding three output images, it can be seen that our method outperforms the other two approaches both in the extraction of the wide line and in the detection of the line structures (see the yellow circles and rectangle). In addition, because our method uses no derivative and the implementation of the circular mask decreases the influence of the directional noise, our wide line detector gives strong noise rejection, that is, produces false crackles caused by reflecting points much less than the other two approaches (see all blue rectangles).

VI. Conclusion and Discussion

This paper presents a novel wide line detector for extracting a whole line by using an isotropic nonlinear filter. Unlike existing approaches, our method employs a hyperbolic secant formula based nonlinear filter to detect the whole of the line. Isotropic

responses are obtained by using a circular mask either with a normalized constant weighting or with a Gaussian profile. The method is robust because of the automatic selection of two parameters—the size of the circular mask and the brightness contrast threshold. The line detection method works very well for a range of images containing lines of different widths, especially for those where the width of lines varies greatly. Because the wide line detector is not dependent on the Gaussian kernel to detect lines, even narrow lines can be extracted well as long as the intensity difference between the narrow lines and the background is larger than the brightness contrast threshold.

Although the proposed line detection method focuses on extracting a whole line, the line position, however, can be easily obtained through a thinning process. Furthermore, the localization of lines via the detection is independent of mask sizes. In addition, the wide line detector is robust against noise because the detection is not based on derivatives of images. Hence, it is effective for practical applications in which noise is inevitable.
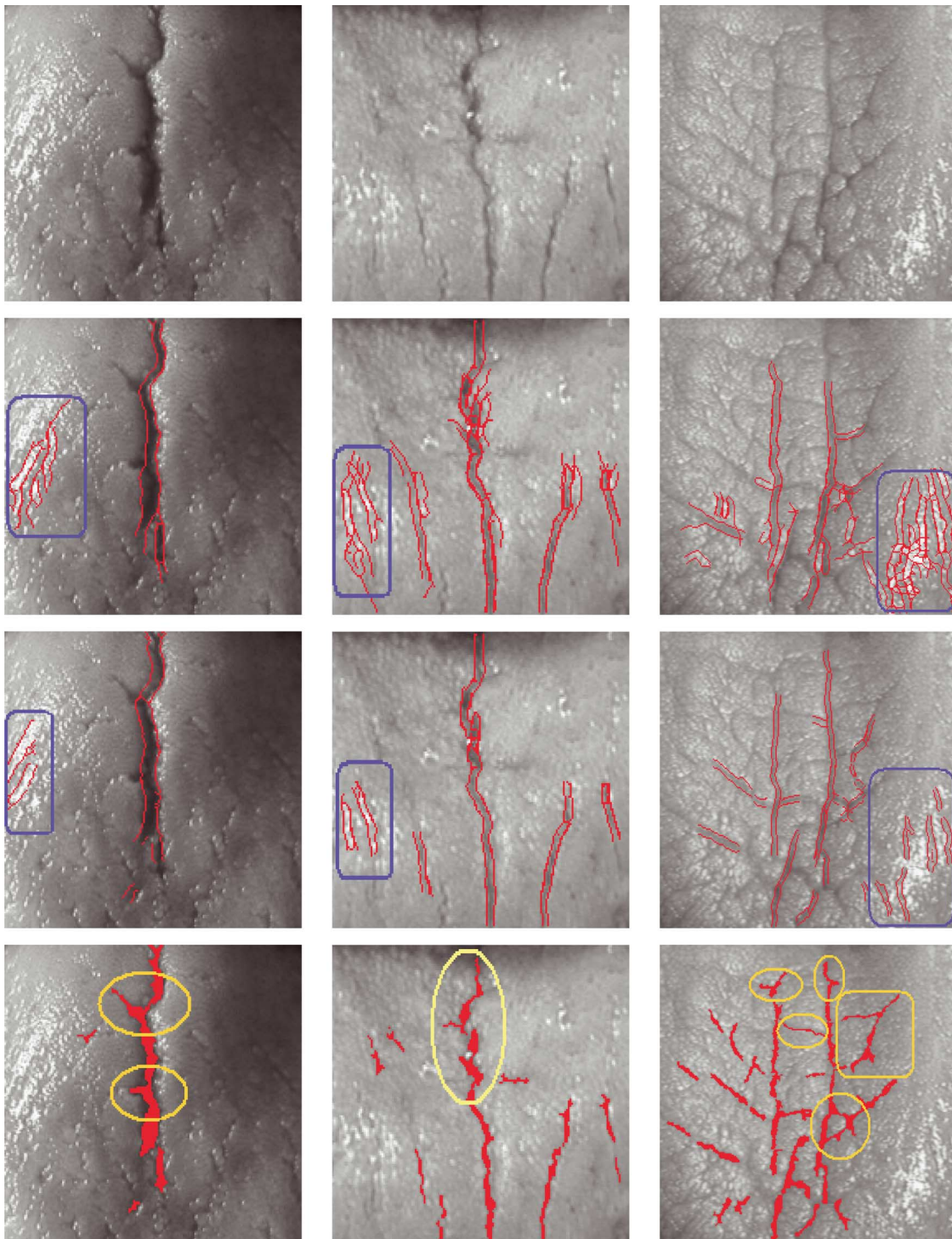
Fig. 11. Segmented (first row) tongue images and (second row) crackle detection results obtained using the edge-based line finder, (third row) the ridge-based line detector, and (last row) the proposed wide line detector. Detected crackles are displayed in red.

The experimental results demonstrate the feasibility and effectiveness of our method.

Finally, it should be pointed out that the proposed method requires the maximum width of lines be estimated before detection, which is not considered in this paper. In our method, if given the maximum width of interested lines, the parameter r is accordingly determined and all lines not wider than this maximum width may be detected as long as they are strong enough.

In order to apply our method fully automatically, our future work is to automatically estimate the maximum line width.

reviewers for their constructive advice and for the revision of the paper.

REFERENCES

[1] D. Behar, J. Cheung, and L. Kurz, "Contrast techniques for line detection in a correlated noise environment," *IEEE Trans. Image Process.*, vol. 6, no. 5, pp. 625–641, Jun. 1997.

[2] G. J. Genello, J. F. Y. Cheung, S. H. Billis, and Y. Saito, "Graeco-Latin squares design for line detection in the presence of correlated noise," *IEEE Trans. Image Process.*, vol. 9, no. 4, pp. 609–622, Apr. 2000.

[3] G. M. Schuster and A. K. Katsaggelos, "Robust line detection using a weighted MSE estimator," in *Proc. Int. Conf. Image Processing*, 2003, vol. 1, pp. 293–296.

[4] H. Li, W. Hsu, M. L. Lee, and H. Wang, "A piecewise Gaussian model for profiling and differentiating retinal vessels," in *Proc. Int. Conf. Image Processing*, 2003, vol. 1, pp. 1069–1072.

[5] E. R. Davies, M. Bateman, D. R. Mason, J. Chambers, and C. Ridgway, "Design of efficient line segment detectors for cereal grain inspection," *Pattern Recognit. Lett.*, vol. 24, pp. 413–428, 2003.

[6] Z. Y. Liu, K. C. Chiu, and L. Xu, "Strip line detection and thinning by RPCL-based local PCA," *Pattern Recognit. Lett.*, vol. 24, no. 14, pp. 2335–2344, 2003.

[7] R. O. Duda and P. E. Hart, "Use of the Hough transformation to detect lines and curves in pictures," *Comm. ACM*, vol. 15, no. 1, pp. 11–15, 1972.

[8] J. Illingworth and J. Kittler, "A survey of the Hough transform," *Comput. Vis., Graph., Image Process.*, vol. 44, pp. 87–116, 1988.

[9] V. F. Leavers, "Which Hough transform?," *CVGIP Image Understand.*, vol. 58, no. 2, pp. 250–264, 1993.

[10] D. H. Ballard, "Generalizing the Hough transform to detect arbitrary shapes," *Pattern Recognit.*, vol. 13, no. 2, pp. 111–122, 1981.

[11] D. Geman and B. Jedynak, "An active testing model for tracking roads in satellite images," *IEEE Trans. Pattern Anal. Mach. Intell.*, vol. 18, no. 1, pp. 1–14, Jan. 1996.

[12] N. Merlet and J. Zerubia, "New prospects in line detection by dynamic programming," *IEEE Trans. Pattern Anal. Mach. Intell.*, vol. 18, no. 4, pp. 426–431, Apr. 1996.

[13] J. H. Jang and K. S. Hong, "Detection of curvilinear structures using the Euclidean distance transform," in *Proc. IAPR Workshop on Machine Vision Applications*, 1998, pp. 102–105.

[14] A. W. K. Loh, M. C. Robey, and G. A. W. West, "Analysis of the interaction between edge and line finding techniques," *Pattern Recognit.*, vol. 34, pp. 1127–1146, 2001.

[15] J. H. Jang and K. S. Hong, "Linear band detection based on the Euclidean distance transform and a new line segment extraction method," *Pattern Recognit.*, vol. 34, pp. 1751–1764, 2001.

[16] D. S. Guru, B. H. Shekar, and P. Nagabhushan, "A simple and robust line detection algorithm based on small eigenvalue analysis," *Pattern Recognit. Lett.*, vol. 25, pp. 1–13, 2004.

[17] J. Canny, "A computational approach to edge detection," *IEEE Trans. Pattern Anal. Mach. Intell.*, vol. 8, no. 6, pp. 679–698, Jun. 1986.

[18] R. M. Haralick, "Ridges and valleys on digital images," *Comput. Vis., Graph., Image Process.*, vol. 22, pp. 28–38, 1983.

[19] J. B. Subirana-Vilanova and K. K. Sung, "Ridge-detection for the perceptual organization without edges," in *Proc. 4th Int. Conf. Computer Vision*, Berlin, Germany, 1993, pp. 57–64.

[20] L. A. Iverson and S. W. Zucker, "Logical/linear operators for image curves," *IEEE. Trans. Pattern Anal. Mach. Intell.*, vol. 17, no. 10, pp. 982–996, Oct. 1995.

[21] A. Busch, "Revision of built-up areas in a GIS using satellite imagery and GIS data," in *Proc. IAPRS*, 1998, vol. 32, pp. 91–98, part 4.

[22] T. Lindeberg, "Edge detection and ridge detection with automatic scale selection," *Int. J. Comput. Vis.*, vol. 30, no. 2, pp. 117–154, 1998.

[23] M. Jacob and M. Unser, "Design of steerable filters for feature detection using canny-like criteria," *IEEE Trans. Pattern Anal. Mach. Intell.*, vol. 26, no. 8, pp. 1007–1019, Aug. 2004.

[24] D. Eberly, R. Gardner, B. Morse, S. Pizer, and D. Scharlah, "Ridges for image analysis," *J. Math. Imag. Vis.*, vol. 4, pp. 353–373, 1994.

[25] T. M. Koller, G. Gerig, G. Szekely, and D. Dettwiler, "Multiscale detection of curvilinear structures in 2-D and 3-D image data," in *Proc. 5th Int. Conf. Computer Vision*, Boston, MA, 1995, pp. 864–869.

[26] C. Steger, "An unbiased detector of curvilinear structures," *IEEE Trans. Pattern Anal. Mach. Intell.*, vol. 20, no. 2, pp. 113–125, Feb. 1998.

[27] J. Chen, Y. Sato, and S. Tamura, "Orientation space filtering for multiple orientation line segmentation," *IEEE Trans. Pattern Anal. Mach. Intell.*, vol. 22, no. 5, pp. 417–429, May 2000.

[28] B. Pang and D. Zhang, "Computerized tongue diagnosis based on Bayesian networks," *IEEE Trans. Biomed. Eng.*, vol. 51, no. 10, pp. 1803–1810, Oct. 2004.

[29] R. Zwiggelaar, S. M. Astley, C. R. M. Boggis, and C. J. Taylor, "Linear structures in mammographic images: Detection and classification," *IEEE Trans. Med. Imag.*, vol. 23, no. 9, pp. 1077–1086, Sep. 2004.

[30] L. Zhang and D. Zhang, "Characterization of palmprints by wavelet signatures via directional context modeling," *IEEE Trans. Syst., Man, Cybern. B, Cybern.*, vol. 34, no. 3, pp. 1335–1347, Jun. 2004.

[31] L. Liu and D. Zhang, "A novel palm-line detector," in *Proc. 5th Int. Conf. Audio- and Video-Based Biometric Person Authentication*, Rye, NY, Jul. 20–22, 2005, vol. 3546, Lecture Notes Comput. Sci., pp. 563–571.

[32] S. M. Smith and J. M. Brady, "SUSAN—A new approach to low level image processing," *Int. J. Comput. Vis.*, vol. 23, no. 1, pp. 45–78, 1997.

Laura Liu received the B.Sc. and M.S. degrees in computer science from the Harbin Institute of Technology, Harbin, China, in 2000 and 2002, respectively. She is currently pursuing the Ph.D. degree in the Department of Computing, The Hong Kong Polytechnic University, Kowloon.

Her research interests include image processing, pattern recognition, and biometrics.

David Zhang (SM'95) graduated in computer science from Peking University, China. He received the M.Sc. degree in computer science and the Ph.D. degree from the Harbin Institute of Technology (HIT), Harbin, China, in 1982 and 1985, respectively, and a second Ph.D. degree in electrical and computer engineering from the University of Waterloo, Waterloo, ON, Canada, in 1994.

From 1986 to 1988, he was a Postdoctoral Fellow at Tsinghua University, China, and then an Associate Professor at the Academia Sinica, Beijing, China. Currently, he is a Chair Professor at the Hong Kong Polytechnic University, Kowloon, where he is the Founding Director of the Biometrics Technology Centre (UGC/CRC) supported by the Hong Kong SAR Government. He also serves as Adjunct Professor at Tsinghua University, Shanghai Jiao Tong University, Beihang University, HIT, and the University of Waterloo. He is the author of more than ten books and 160 journal papers.

Prof. Zhang is a Croucher Senior Research Fellow, Distinguished Speaker of the IEEE Computer Society, and a Fellow of the International Association of Pattern Recognition (IAPR). He is the Founder and Editor-in-Chief of the *International Journal of Image and Graphics* (IJIG); an editor of a book in the Springer International Series on Biometrics (KISB); an organizer of the International Conference on Biometrics Authentication (ICBA); an Associate Editor of more than ten international journals, including the IEEE TRANSACTIONS ON SYSTEMS, MAN, AND CYBERNETICS—PART A: SYSTEMS AND HUMANS, the IEEE TRANSACTIONS ON SYSTEMS, MAN, AND CYBERNETICS—PART C: APPLICATIONS AND REVIEWS, and *Pattern Recognition*; and Technical Committee Chair of IEEE CIS.

Jane You (M'95) received the B.Eng. degree in electronic engineering from Xi'an Jiaotong University, Xi'an, China, in 1986, and the Ph.D. degree in computer science from La Trobe University, Melbourne, Australia, in 1992.

From 1993 to 1995, she was a Lecturer with the School of Computing and Information Science, University of South Australia. From 1996 to 2001, she was with the School of Computing and Information Technology, Griffith University, Brisbane, Australia, where she held the positions of Lecturer and Senior Lecturer. She joined the Department of Computing, Hong Kong Polytechnic University, Kowloon, in 1999, where she is currently an Associate Professor. Her research interests include visual information retrieval, image processing, pattern recognition, multimedia systems, biometrics computing, and data mining.

Dr. You was awarded a French Foreign Ministry International Fellowship in 1993.